Diamond & Related Materials 168 (2026) 113981

Contents lists available at ScienceDirect

Diamond & Related Materials

journal homepage: www.elsevier.com/locate/diamond

Identification of boron-related traps via capacitance spectroscopy in diamond Schottky diodes☆

Giacomo Biasin [a,f,*], Manuel Fregolent [a,f], Matteo Buffolo [a,b,f], Carlo De Santi [a,f], Julien Bassaler [c], Vishwajeet Maurya [c], Juliette Letellier [c], Gaudenzio Meneghesso [a,f], Enrico Zanoni [a,f], Giovanni Verzellesi [d,f], Alessandro Chini [e,f], Matteo Meneghini [a,b,f]

[a] Department of Information Engineering (DEI), University of Padova, 35131, Padova, Italy
[b] Department of Physics and Astronomy (DFA), University of Padova, 35131, Padova, Italy
[c] DIAMFAB, 38600, Fontaine, France
[d] Department of Sciences and Methods for Engineering (DISMI), University of Modena and Reggio Emilia, 42121, Reggio Emilia, Italy
[e] Department of Engineering "Enzo Ferrari", University of Modena and Reggio Emilia, 41125, Modena, Italy
[f] National Interuniversity Consortium for Nanoelectronics (IU.NET), Italy

ARTICLE INFO

Keywords:
Defect spectroscopy
Diamond
Schottky diode
Boron
Deep levels

ABSTRACT

We present a comprehensive investigation of boron-related trapping phenomena in diamond Schottky diodes based on capacitance-voltage (C—V) measurements and isothermal capacitance transient spectroscopy (ICTS). The C—V characteristics exhibit a pronounced hysteresis, whose magnitude increases with temperature, thus indicating the presence of temperature-activated charge trapping within the depletion region. ICTS measurements reveal the presence of two distinct trapping processes. The faster process exhibits an activation energy of (0.39 ± 0.02) eV and an unconventional apparent capture cross-section of 1.9×10^{-20} cm^2. The extracted activation suggests that the trap is related to substitutional boron. By varying the filling time, we observed an emission process that follows a stretched exponential trend, which is ascribed to a distribution of trap levels. The characterization of the dynamic behavior of boron-related traps with temperature is highly relevant for studying the dynamic properties of diamond-based Schottky-barrier diodes and transistors.

1. Introduction

Diamond is an ultra-wide-bandgap semiconductor (5.47 eV) characterized by high hole mobility, exceptional thermal conductivity, and an extremely high breakdown electric field, making it a strong candidate for high-power and high-frequency device applications [1,2]. For diamond-based semiconductor devices, among the most common dopants in diamond, boron acts as the shallowest acceptor with an activation energy of approximately 0.38 eV [3–5], whereas nitrogen and phosphorus behave as deep donors with activation energies near 1.7 eV and 0.58 eV, respectively [6,7]. The high activation energy of n-type dopants results in a non-trivial fabrication of high-performance p-i-n diodes [8]. As a consequence, current research increasingly focuses on unipolar Schottky-barrier diodes, which already demonstrated breakdown voltages exceeding 1 kV [9,10] and offer a more feasible route toward high performance diamond power devices. For these devices, low-doping concentration, to sustain higher breakdown voltages in the drift region, and low-resistivity layers, to reduce ON-state losses in the contact region, are desired.

Deep-levels associated to intrinsic and extrinsic defects can worsen the device performance and be particularly detrimental to both DC and switching applications, where the dynamics of charge trapping and detrapping processes may pose a limit to the operating frequency. Moreover, since dopants with large activation energies remain only partially ionized at standard operating temperatures, additional transient effects may arise from the trapping or release of carriers, potentially reducing the effective breakdown voltage of UWBG devices [11,12].

Capacitance Deep-Level Transient Spectroscopy (C-DLTS) [13] can be effectively employed to identify deep-levels and to extract their characteristic parameters, such as the activation energy E_A, the capture cross-section σ and the defect density N_T. Due to limitations in

☆ This article is part of a Special issue entitled: 'ICDCM2025' published in Diamond & Related Materials.

* Corresponding author at: Department of Information Engineering (DEI), University of Padova, 35131, Padova, Italy.
E-mail address: giacomo.biasin@phd.unipd.it (G. Biasin).

https://doi.org/10.1016/j.diamond.2026.113981
Received 4 March 2026; Received in revised form 14 July 2026; Accepted 17 July 2026
Available online 19 July 2026
0925-9635/© 2026 Published by Elsevier B.V.

measurement time and temperature, C-DLTS can probe only the shallower part of the bandgap [14]; however, the traps identified in this way can still be responsible for performance worsening during switching operations. Therefore, to probe for deeper traps, optical spectroscopy, such as DLOS, is preferred [15].

Taking as an example Schottky-barrier diodes (SBDs) that are intrinsically designed for high-speed operation, these defects can exhibit unusually slow capture and emission kinetics depending on the trap characteristic parameters. These slow processes can conflict with the inherently fast switching behavior of the diode degrading the overall dynamic performance. Guo et al. demonstrated that, in polycrystalline diamond Schottky diodes, slow trap kinetics characterized by carrier capture and emission time constants on the order of tens of seconds can significantly modify the current-voltage characteristics. These slow processes delay the reaching of steady-state conditions during measurements, thereby limiting the straightforward use of diodes that exhibit such trap dynamics [16]. Analogously, Nikolenko et al. demonstrated, in Schottky diodes fabricated from monocrystalline diamond, that deep-level defects can modify both the Schottky barrier height and the ideality factor as a function of the respective trap occupancy. [17]. Moreover, the presence of slow trap kinetics and trapped charge can further degrade the blocking capabilities, particularly in devices designed to withstand high electric fields on the order of several megavolts per centimeter (MV/cm). In addition, a detailed analysis of trap kinetics is essential for Technology Computer-Aided Design (TCAD) simulations, as it enables more accurate calibration of physical models for diamond-based power devices. With respect to slow dopant ionization and the activation of slow traps under high electric-field conditions, Kah et al., using TCAD simulations of Schottky barrier diodes (SBDs), demonstrated that under fast switching conditions the delayed response of these centers can reduce the effectiveness of the junction termination [11]. An analogous behavior was reported for another wide-bandgap semiconductor, namely silicon carbide (SiC) [18,19].

To date, capacitance- and current-based DLTS techniques applied to boron-doped Schottky-barrier diodes and similar structures have primarily identified deeper traps, with activation energies between 0.7 and 1.6 eV with respect to the valence band [20,21].

This work aims to investigate trapping phenomena related to relatively shallow, yet dynamically slow, traps boron-doped diamond Schottky diodes. By combining capacitance against voltage (C—V) analysis with isothermal capacitance transient spectroscopy (ICTS) [22], we have analyzed extended measurement windows with the objective of identifying the underlying defect processes and evaluating their impact on device behavior. The spectroscopic characterization of this class of defects in ultra-wide-bandgap materials will facilitate future investigations of their macroscopic impact and degradation behavior under realistic operating conditions, thereby enabling the optimization of diamond-based devices such as field-effect transistors (FETs).

Samples under test are described in Section 2. Employed measurement methodologies are described in Section 3 with a focus on the use of stretched exponentials to rigorously fit the stretched-exponential capacitance transients due to non-idealities. Results from C—V characteristics and ICTS are reported in Sections 4. Finally, in Section 5, we have compared our extracted trap signatures with currently available literature reports for traps in monocrystalline diamond-based devices.

2. Sample description

The devices under test consist of pseudo-vertical p-type Schottky-barrier diodes manufactured on a low-Boron doped layer. Homoepitaxial layers were grown on 500-μm-thick 4 × 4 mm^2 high-pressure high-temperature (HPHT) substrate by microwave plasma-assisted chemical vapor deposition (MPCVD). First, a 520 nm heavily boron-doped p^{++} ([B] > 3 × 10^{20} cm^{-3}, over the metal-insulator transition) layer is grown, to enhance the formation of ohmic contact and enable lateral current transport. Then, a 2860 nm p^- layer with an effective boron concentration of about 10^{16} cm^{-3}, extracted from C—V measurements, has been grown as the main drift layer.

In this sample, each diode is isolated from its neighboring with a deep etching going through the insulating substrate. Afterwards, a molybdenum-based Schottky contact is deposited on top of the p^- layer, and the ohmic contact is made by deposition of Ti on the p^+ layer.

The schematic cross-section of a single diode is shown in Fig. 1.

3. Experimental methods

The setup employed in this work is custom-made for this purpose and it consists of several instruments connected as shown schematically by Fig. 2 (a), and it is controlled by a computer software. The main instrument in this setup is the Boonton 7200, a fast capacitance meter that operates at a frequency of 1 MHz, to which an external bias voltage can be applied. Instead, the other instruments are a conventional arbitrary waveform generator (AWG) and a digital storage oscilloscope (DSO). The constant bias waveforms were generated by the AWG and then amplified in order to increase the maximum rate of output current variation. The capacitance meter superimposes a 50 mV AC signal to sense the capacitance of the DUT, which is provided as an analog voltage output. The resulting bias voltage and capacitance-output waveforms were sampled by the DSO. The acquired time windows were subsequently averaged to reduce the noise contribution.

To evaluate the behavior in function of temperature, the sample was tested inside a cryogenic probe station, in vacuum conditions and under dark.

The samples were initially tested with “go” and “back” C—V characteristics (from −10 V to 0 V and backward) at different temperatures between 240 K and 300 K. The presence of hysteresis between the two curves indicates that traps are responding to the change in carrier concentration in the depletion region. For instance, trapping of majority carriers $p_T(t)$ will shift the C—V characteristic, as explained by Eq. (2), by reducing the net charge in the depletion region $N_{SCR} = N_A - p_T$, where p_T is the trapped majority-carrier charge concentration, thus decreasing the capacitance at the same bias voltage. The C—V characteristic is also helpful as a preliminary step before the ICTS to define the operative condition for subsequent measurements. From this characteristic, it is possible to test the dimension of the depletion region that will be swept during the ICTS and also the apparent free hole concentration in that region.

Then, ICTS was performed within the same temperature range. ICTS was employed to better manage the duration of the measurement transients, which do not reach saturation in the selected time window of 1000 s, and their non-ideal exponential shape. Under these conditions, a DLTS temperature-scan would be experimentally impractical due a) to the long acquisition times required to maintain adequate temperature resolution, or b) to the extremely high temperatures required to accelerate the transients. The ICTS method [18] is based on the classical C-DLTS signal structure [13], which is divided into three phases: (i) prefill, (ii) filling and (iii) measurement, as shown in Fig. 2 (b). The (i) initial prefill is implemented to establish a reproducible condition before the

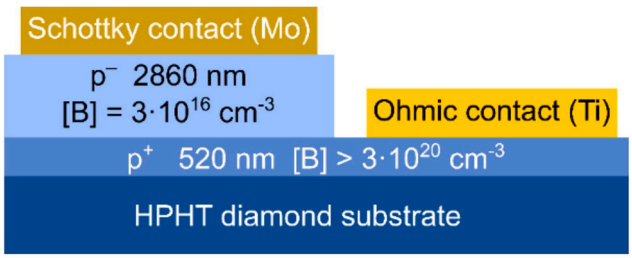


Fig. 1. Schematic cross-section of the pseudo-vertical Schottky diodes under investigation.

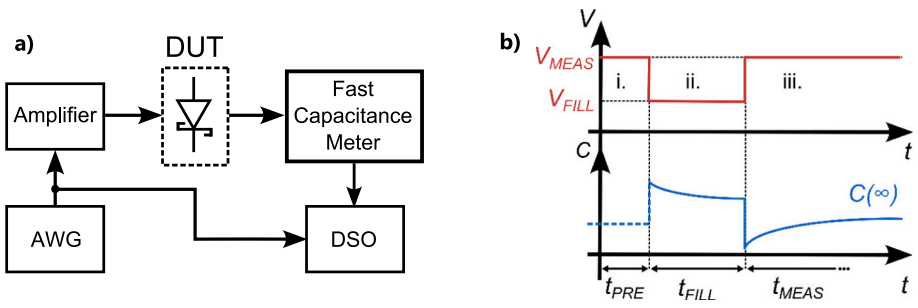


Fig. 2. (a) Schematic of the setup used to extract the C—V characteristics and to perform the ICTS. (b) Ideal waveforms of the bias voltage and AC capacitance during the ICTS.

filling phase. During this stage, the device is held at the same voltage in the measurement phase for a shorter period of time. This step is technically required because during the setup of the instrumentation before each transient analysis, the bias is automatically reset to 0 V. Since the duration of this zero-biased state can vary, the subsequent stabilization phase ensures that the device reaches a consistent equilibrium state before the start of the actual transient acquisition. Then, the (ii) filling phase is used to shrink the depletion region and to fill the traps previously located close to the edge of the space charge region (SCR). Afterwards, the bias is restored to the measurement value: this induces a change in the charge state of both dopants and traps, the latter of which results in a measurable and relatively slow temperature-dependent transient in the capacitance of the device.

In this work, we performed the filling phase at 0 V to avoid exciting minority-carrier traps, and we used a measurement bias of 2 V, balancing between the need for a visible transient and the reduction of field effects. The temperature range used for the ICTS measurements, which was also adopted for the C—V characterization, was selected to match the emission transients of the trapping processes with the temporal resolution of the acquisition system employed. This consideration was particularly critical in cases where the transients contained multiple processes with time constants differing by several orders of magnitude, simultaneously requiring both long acquisition windows and fine temporal resolution. The use of higher temperatures would have shifted the emission rates of the faster traps beyond the sampling capabilities of the system, resulting in a loss of information.

3.1. Capacitance transient fitting function

Traditionally, the junction capacitance per unit area of an SBD is given by [23]:

$$C(V) = \sqrt{\frac{q\,\varepsilon\,N_{SCR}}{2|V_{bi} - V|}}\,, \tag{1}$$

in which $\varepsilon = 5.7\,\varepsilon_0$ is the dielectric constant of diamond and ε_0 is the vacuum permittivity, N_{SCR} is the net fixed charge inside the depletion region (almost equal to the ionized acceptor concentration N_A in case of low concentration of defects), V_{bi} is the built-in voltage of the junction and V the bias voltage.

In the presence of electrically active traps, the time-dependent trapped charge density $p_T(t)$ partially compensates the ionized acceptors, thereby modifying the effective space charge density within the depletion region; in that case, the effective space charge within the SCR is $N_{SCR} = N_A - p_T(t)$ and the previous equation modifies as follows

$$C(V,t) = \sqrt{\frac{q\varepsilon(N_A - p_T(t))}{2|V_{bi} - V|}}\,. \tag{2}$$

At the end of the transient related to measurement phase, the traps would have ideally emitted all the trapped holes, and so their contribution would go to zero, i.e. $p_T(\infty)\to 0$. Therefore, we can define the steady-state capacitance $C_\infty(V) = \sqrt{q\,\varepsilon\,N_A/(2|V_{bi} - V|)}$.

Furthermore, we can consider a distribution of N non-interacting traps, each defined by a specific energy level and capture cross-section, thus a distinct time constant τ_i. For each trap level i, we can consider the solution of the generation-recombination rate equation $dp_{T,i}/dt = -\tau_i^{-1} p_{T,i}$ at that level for a highly ionized depletion region, where the capture rate can be ignored. In this condition the trap level will be entirely filled at $t = 0$, resulting in $p_{T,i}(0) = N_{T,i}$, and for $t\to\infty$, all trapped charge will be emitted, hence $p_{T,i}(\infty)\to 0$. Therefore, the solution of the rate equation can be described as

$$p_{T,i}(t) = N_{T,i}\exp\left(-\frac{t}{\tau_i}\right). \tag{3}$$

For multiple non interacting trap levels, the individual exponential emission components (3) can be summed and inserted into the general capacitance expression (2), yielding a composite transient that reflects the combined contribution of all trap states as

$$C(t) = C_\infty\sqrt{1 - \sum_i^M \frac{p_{T,i}(t)}{N_A}}. \tag{4}$$

When the trap concentration is significantly lower than the ionized acceptor density, i.e. $N_{T,i}/N_A \ll 1$ for all traps, the capacitance expression can be linearized, resulting in the well-known first order approximation for the transient response,

$$C(t) = C_\infty\left(1 - \frac{1}{2}\sum_i^M \frac{p_{T,i}(t)}{N_A}\right). \tag{5}$$

In case of spatially or energetically distributed traps, we can associate tightly packed trap levels as band of defects defined by a finite continuous distribution of time constants, which empirically results in the observation of stretched, rather than purely, exponential capacitance transients [24,25] as

$$p_{T,k}(t) = N_{T,k}\exp\left(-\left(\frac{t}{\tau_k}\right)^{\beta_k}\right), \tag{6}$$

where the stretching exponent β_k determines the deviation of the transient from a pure exponential (for the trap band k), and so for $\beta_k \le 1$, it will result in a longer transient than for the ideal case [21]. Each trap band is then defined by the central time constant τ_k and by the width of the band that is described by the stretch factor β_k. In the limiting case that the band is defined by a single distinct trap level, (6) can be reduced to (3) by setting the stretching factor as $\beta_k = 1$.

When only the rising portion of the transient, in the vicinity of its τ_0, lies within the measurement window, the response can be approximated by a logarithmic dependence on time reflecting the behavior of a very broad trap distribution. The latter contribution is then taken out from the square-root term and so as

$$C(t) = C_\infty \left[\sqrt{1 - \sum_k \frac{p_{T,k}(t)}{N_A}} - m \ln\left(\frac{t}{\tau_0}\right) \right] , \quad (7)$$

where m and τ_0 are the fitted slope and time constant for the logarithmic part of the transient [14,22].

The emission rate τ_p^{-1} depends on the effective density of states in the valence band N_V and on the thermal velocity of holes v_{th}, which are both temperature dependent quantities determined by the effective mass m_h and fundamental constants along with trap characteristic activation energy E_A and capture cross-section σ_p as [26].

$$\tau_p^{-1} = \frac{\sigma_p v_{th} N_V}{g_A} \exp\left(-\frac{q}{k_B T} E_A \right), \quad (8)$$

where $N_V(T) = \left[2(2\pi m_h k_B)^{3/2} h^{-3}\right] \cdot T^{3/2}$ [27] with $m_h = 0.908\, m_0$ [28] and $g_A = 4$ the degeneracy factor [1,5], $v_{th}(T) = \sqrt{3k_B/m_h}\, T^{1/2} = T^{1/2} \bullet 7.08 \times 10^5$ cm s^{-1} K$^{-1/2}$.

Rewriting (8) to exploit the temperature dependence as in Arrhenius plot, we obtain a linear trend whose slope provides the activation energy E_A and from the intercept y_0, it is possible to extract the apparent capture cross-section σ_p as

$$\sigma_p = K_{\sigma_p} \exp(-y_0), \quad (9)$$

where $K_\sigma = h^3 / \left(2\, g_A\, m_h\, k_B^2 \sqrt{3(2\pi)^2}\right) = 8.45 \times 10^{-23}$ cm^2 s^{-1} K^{-1}.

4. Results

4.1. Capacitance - voltage characteristics

Fig. 3 (a) shows the measured C—V characteristics, where at the lowest temperatures (240 K) the dopant starts to reach the freeze-out regime, resulting in a substantial expansion of the depletion region and almost no capacitance change for higher reverse voltages, i.e., toward 10 V. Consequently, the lower bound of the temperature range for the ICTS measurements was set to 250 K in order to ensure a sufficiently large capacitive transient amplitude for reliable results. By evaluating the apparent dopant profile from the C—V characteristics, as shown in Fig. 3 (c), we found that the estimated net charge $N_A - N_D$ is almost constant over the tested voltage range. For the subsequent ICTS measurements, we kept the voltage sweep in the range [0,2] V, which is equivalent to a depletion region between 360 nm and 1800 nm. In the same depletion region range at $T = 300$ K the apparent free charge concentration is 1.1×10^{16} cm^{-3}, on average. On the other hand, the visible hysteresis exhibited by the C—V characteristics, whose area depends on temperature, as highlighted in the representative C—V characteristics in Fig. 3 (b), suggests the presence of a trap-related capture-emission phenomenon.

4.2. Isothermal capacitance transients spectroscopy

To investigate the trapping process highlighted from the hysteresis of the C—V measurements, we decided to carry out additional ICTS measurements by using a fill pulse at 0 V for 500 s, and a measurement voltage of 2 V, as described in Section 3. We repeated the capacitance

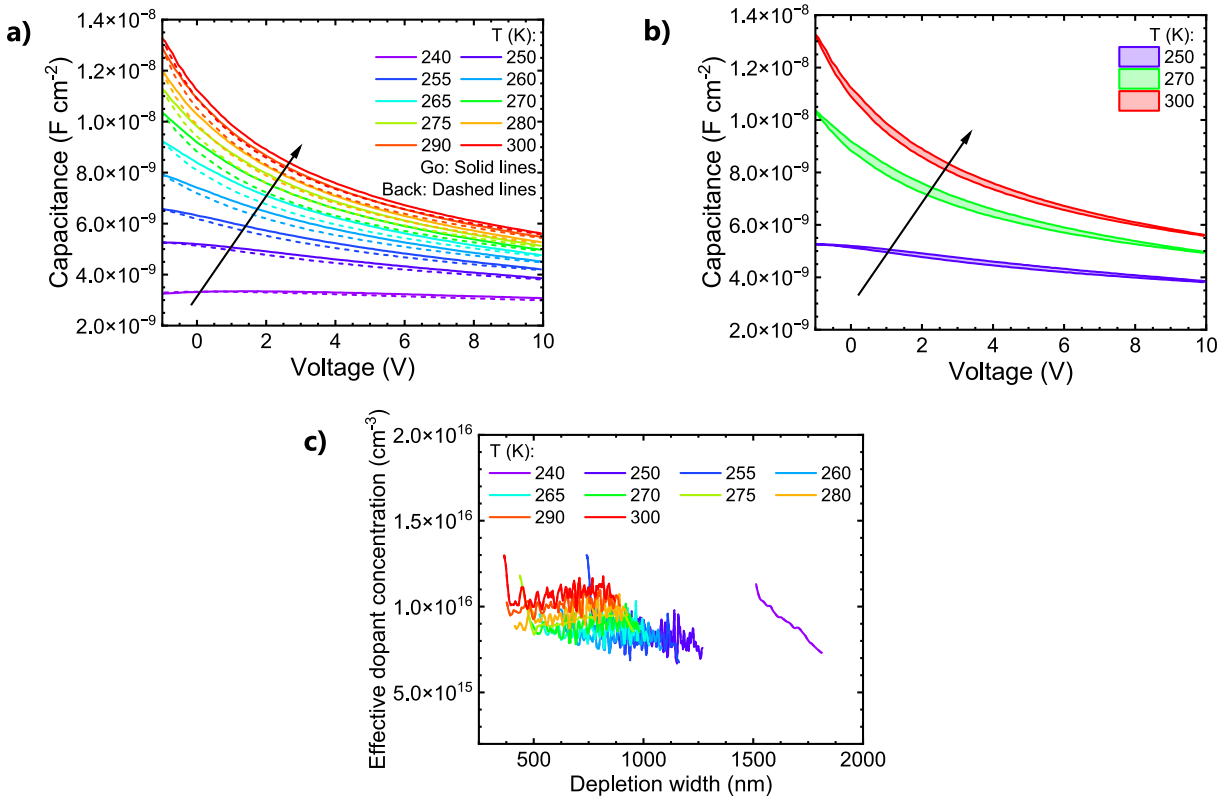


Fig. 3. (a) Capacitance versus voltage characteristics of the diode repeated at different temperatures. The solid lines represent data derived from the "go" sweep, whereas the subsequent "back" direction is shown with a dashed line. (b) Representative C—V characteristics from (a), with the enclosed area associated with the hysteresis between the "go" and "back" sweeps highlighted. (c) Effective dopant concentration against depletion region as extracted from the C—V characteristics.

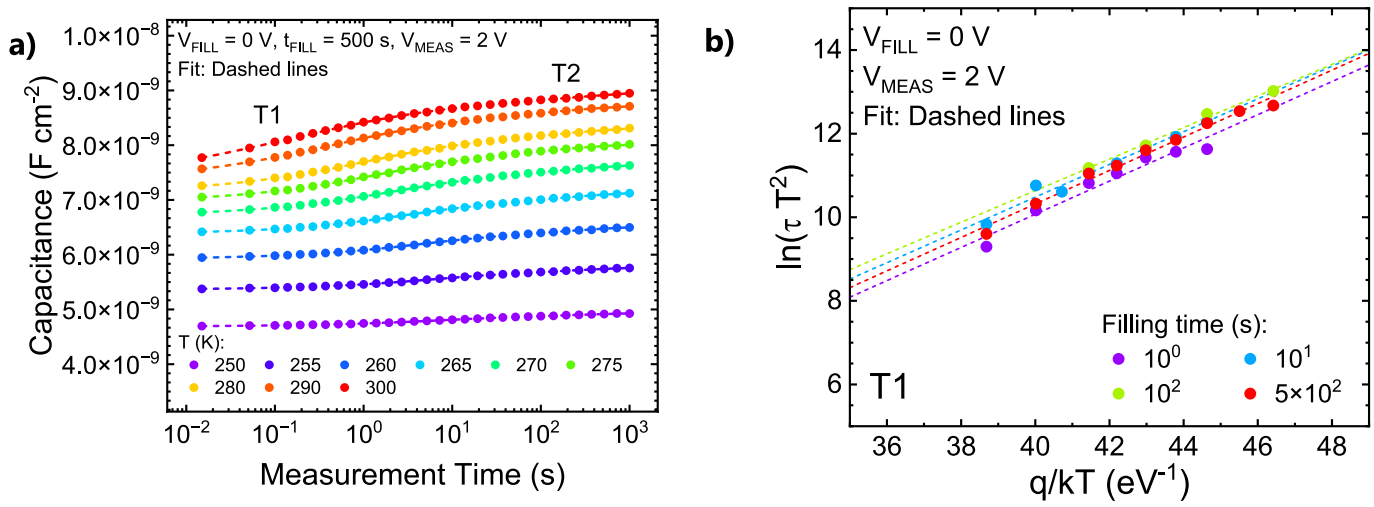


Fig. 4. (a) Capacitive transients plotted against time as dots, at different temperatures, for the measurement phase. The dashed lines are the fit of the transients assuming two traps: T1 and T2. (b) Arrhenius plot of the logarithm of the fitted trap time constant multiplied by the square of the temperature $ln(\tau\, T^2)$ against q/kT, for process T1. The measurements were repeated at different filling times.

transients from 250 K to 300 K, as shown in Fig. 4(a). The duration of the filling pulse employed for this measurement was selected to ensure complete trap occupancy, and insights on the impact of the filling pulse duration are presented in Section 4.3, whose filling pulses are shown in Fig. 5 (a).

The peculiar capacitance transients indicate the presence of two processes, due to the two changes in slope visible in the majority of the transients. The faster process (T1) exhibits a stretched exponential behavior, while the slower process (T2) does not fully saturate within the measurement window and partially overlaps with T1. Consequently, we employed a two-term stretched exponential function to fit the transient response, thereby enabling the extraction of the characteristic parameters.

Because the slower transient T2 does not reach steady state in the selected measurement window and its amplitude cannot be assumed to be negligible, the full capacitance expression, i.e. Eq. (4), was employed for fitting, rather than the linear approximation valid only for small trap concentrations. At the same time, the approximation of the logarithmic transient, as in Eq. (7), cannot be applied without losing information, since the transients are not fully logarithmic over the whole temperature range. The parameters extraction for T2 is affected by its low stretch factor and by the overlapping with T1. Due to these reasons, the accuracy of the fitted time constant is reduced and a description of this phenomena can only be done qualitatively. Therefore, we focused on the results from the first process T1 that showed an activation energy E_A of 0.40 eV with t_{FILL} = 500 s, comparable with the expected one for the boron dopant.

ICTS measurements were repeated for various filling times in the range from 10^0 s to 10^2 s, and the extracted time constants were analyzed through Arrhenius plots, as shown in Fig. 4(b), to determine the variation activation energy and capture cross section associated with T1. The extracted parameters are also reported in the Table 1. From those results, we can notice that the filling time does not play a significant role for time longer than 1 s, since the variations in activation energy and capture cross-section are quite limited.

Generally, from ICTS measurements, the trap concentration for each trap level can be extracted directly from the capacitive transients using the fitted initial value $C_{0,k}$ and transient amplitude $C_{\infty,k}$ to isolate the single transient. If the overall initial steady-state value can be estimated from the capacitive transients, the accuracy of these two parameters is

Table 1
T1 activation energy and capture cross-section as extracted from the Arrhenius plot reported in Fig. 4(b).

Filling time, t_{FILL} (s)	10^0	10^1	10^2	5×10^2
Activation energy, E_A (eV)	0.40 ± 0.04	0.39 ± 0.03	0.38 ± 0.02	0.40 ± 0.02
Capture cross-section, σ (cm^{-2})	2.8×10^{-20}	1.5×10^{-20}	7.5×10^{-21}	2.5×10^{-20}

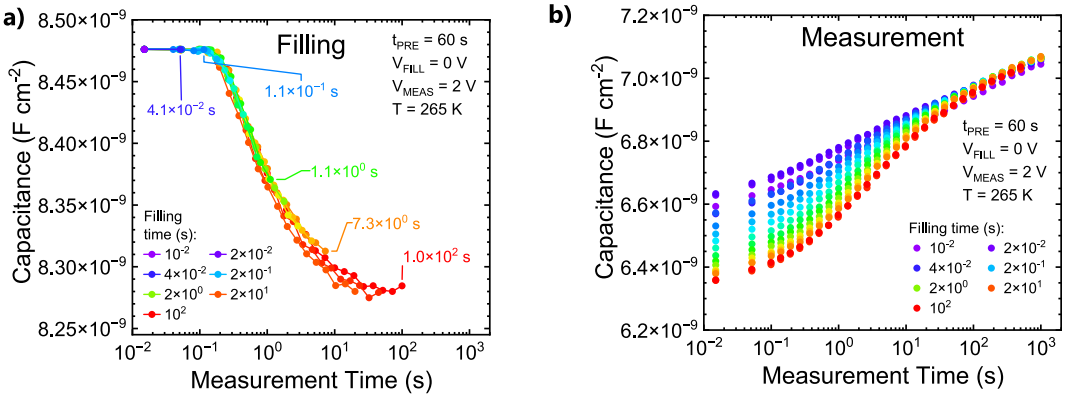


Fig. 5. Capacitive transients against logarithmic time during filling (a) and measurement (b) phase at different filling times. The labels in (a) are used to highlight the end of the transient for the respective filling time.

high enough. In that case, by combining (4) and (6) for $t = 0$ and $t \to \infty$, the trap concentration can be extracted as $p_{T,k}/N_A = 1 - \left[(C_{0,k} - C_{\infty,k})/C_{\infty,k}\right]^2$. However, in this case, since the transients of T1 and T2 are superimposed, the initial (C_0) and final (C_∞) capacitance values cannot be isolated reliably, preventing an accurate determination of the trap to dopant concentration ratio. In any case, the average fitted trap to dopant concentration ratio $p_{T,1}/N_A$ for T1 is about 11%. In addition, the stretch factor β for T1 is almost constant with the filling time and slightly decreasing with temperature around (0.5 ± 0.1), meaning that the traps that arises to process T1 are quite spread.

4.3. Impact of filling time

To evaluate the change in the relative impact of T1 and T2 under different filling conditions, we repeated the ICTS measurement, varying the filling time logarithmically from 10^{-2} s to 10^{2} s and fixing the temperature at $T = 265$ K, where both transients are especially visible.

After the prefilling phase, the sample was always brought to the same condition, as testified by the completely superimposable filling transients reported in Fig. 5 (a). Analysis of the filling transient reveals the emergence of a dominant trapping mechanism for filling times longer than approximately 1.1×10^{-1} s, as evidenced by a pronounced increase in the amount of captured charge, as shown by the filling transients in Fig. 5 (a).

On the other hand, for filling times shorter than approximately 4.1×10^{-2} s, the transient associated with T2 becomes dominant, while the contribution of T1 is comparatively weaker in the measurement transients reported in Fig. 5 (b). In this condition, the kinetic of process T2 results almost logarithmic, therefore, by leveraging the relation reported in Eq. (7), the capacitance transient related to T1 can be isolated and analyzed by simply subtracting the effect of T2. In addition to that, from Fig. 5 (b) we can also observe that (i) there is almost no variation in the final values of the measurement transients, whereas there is a decrease in their initial value at increasing filling time, and that (ii) the slope of the transient for $t > 200$ s is almost the same since the fitting parameters m and τ_0 are almost constant over the tested filling time range.

These results indicate that a) the kinetics and amplitude of T2 are largely insensitive to filling time variations, whereas b) the filling transient primarily reflects the capture dynamics associated with T1.

5. Comparison with literature

The trapping process T1 was found to have an average activation energy $\overline{E}_A$ of (0.39 ± 0.02) eV and an unconventional apparent capture cross-section $\overline{\sigma}_p$ of 1.9×10^{-20} cm^{-2}, whose results are compared in Fig. 6 to other DLTS-detected traps in the monocrystalline B-doped diamond layer found in the literature. The calculated activation energy value is comparable to that of substitutional boron, which is about 0.38 eV [3–5]. The apparent cross-section, on the other hand, appears to be rather smaller than the one expected from the boron dopant; consequently, some considerations can be made. In general, the capture cross-section is related to the nature of the trap, and so it can take values from about 10^{-12} cm^2, for Columbic attractive centers, such as acceptor-like traps for holes, to about 10^{-20} cm^2 or less for repulsive centers, as donor-like traps. In the case of substitutional boron in diamond, the capture cross-section was estimated by other non-DLTS-based methods, such as capture lifetime after photoexcitation, in the range between 10^{-14} cm^2 and 10^{-13} cm^2 [29,30], as expected for an acceptor-level [26]. It is well accepted that cross-section values extracted from Arrhenius plots can have uncertainties of several orders of magnitude, due to several factors, for example: a) cross-talk between defects having similar activation energies and different capture rates [31]; b) changes in the emission rate induced by electric-field [32]; c) impact of Fermi level position on the accuracy of extracted trap parameters [33]. On top of this, substitutional boron is not the only boron-related trap present in B-doped diamond, and other B-related complexes (e.g., boron clusters, complexes with interstitial hydrogen, BH_2, etc.) may be present in high concentrations [34–36]. With the information obtained within this study, a definitive conclusion on the origin of the found trap T1 cannot be given; however, the proximity of the T1 activation energy to that of the substitutional boron, and the large density (11% of the dopant) suggests that this process is related to the boron-related defects inside the device.

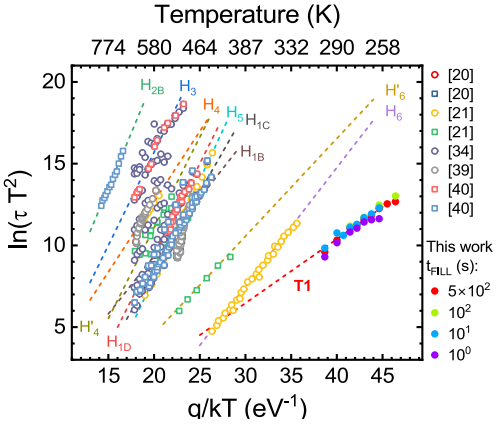


Fig. 6. Comparison of other DLTS-detected traps in monocrystalline B-doped diamond layer [20,21,34,39,40], in open dots, and the one found in this work, T1, in full dots. Circles are used to mark capacitance-based measurements, and squares for current-based ones. The dashed lines are based on the nomenclature of the found traps [34].

Finally, in relation to the slower process T2, since its transient was not entirely visible in the chosen time window, it is not trivial to properly characterize and identify the related defects. Despite this, under the tested conditions, T2 exhibited markedly stretched-exponential behavior, which may be related to a distributed interacting defect, such as a dislocation [37,38].

6. Conclusions

With this work, we analyzed the trapping processes visible at room temperature in boron-doped diamond Schottky-barrier diodes, with additional emphasis on the characterization of non-ideal trap dynamics and the presentation of a methodological analytical framework based on the stretched exponential formalism.

Hints of ongoing trapping were first noticed by go and back C—V characteristics that showed hysteresis, whose magnitude increased with temperature. In addition, the doping profile was found to be nearly constant at approximately 1.1×10^{16} cm^{-3}, at $T = 300$ K, over the area swept by the ICTS.

Further analyses using ICTS revealed two trapping processes: a faster one, T1, and a slower one, T2, the latter exhibiting nearly logarithmic behavior. Therefore, stretched exponentials were used to track the non-idealities of both transients, and we repeated ICTS measurements in different filling time conditions, focusing on the transient related to T1. Filling-time-dependent ICTS revealed that the amplitude of the filling transient is related to the amplitude of the capacitance transient by T1 in the measurement phase, which is proportional to the quantity of trapped holes.

T1 showed an activation energy of (0.39 ± 0.02) eV, which is closed to the one of the substitutional boron, and an apparent capture cross-section of 1.9×10^{-20} cm^{-2}. Under the tested conditions, trap T2 behaved similarly to a distributed or interacting defect.

It is worth noticing that the identification of boron-related signatures, such as the T1 trap, underscores that slow trapping mechanisms detrimental to device performance can originate from intentional dopants rather than exclusively from external contamination or intrinsic defects. Furthermore, a substantial trap occupancy at room-temperature is expected to affect dynamic device parameters, such as on-resistance,

through capture and emission processes occurring on timescales consistent with those characterized in this work, as in Fig. 5(a). This finding highlights an intrinsic challenge in diamond-based electronics, where the very species incorporated to enhance functionality may simultaneously promote the formation of performance-limiting defects.

With this work, we have found two new processes visible at room temperature in boron-doped diamond Schottky diodes, of which one suggests a relation with the substitutional boron, with a significant impact on device capacitance. Furthermore, we proposed a revised analysis of the capacitive transients for the ICTS method.

CRediT authorship contribution statement

Giacomo Biasin: Writing – review & editing, Writing – original draft, Methodology, Investigation, Formal analysis, Data curation, Conceptualization. **Manuel Fregolent:** Writing – review & editing, Supervision, Methodology, Formal analysis, Data curation, Conceptualization. **Matteo Buffolo:** Writing – review & editing, Supervision, Methodology, Formal analysis, Data curation, Conceptualization. **Carlo De Santi:** Writing – review & editing, Supervision, Methodology, Formal analysis, Data curation, Conceptualization. **Julien Bassaler:** Writing – review & editing, Supervision, Resources. **Vishwajeet Maurya:** Writing – review & editing, Supervision, Resources. **Juliette Letellier:** Writing – review & editing, Supervision, Resources. **Gaudenzio Meneghesso:** Project administration, Funding acquisition. **Enrico Zanoni:** Project administration, Funding acquisition. **Giovanni Verzellesi:** Writing – review & editing, Supervision. **Alessandro Chini:** Writing – review & editing, Supervision. **Matteo Meneghini:** Writing – review & editing, Supervision, Methodology, Formal analysis, Data curation, Conceptualization.

Declaration of competing interest

The authors declare that they have no known competing financial interests or personal relationships that could have appeared to influence the work reported in this paper.

Acknowledgments

This work was funded by the European Union, through the “European Climate, Infrastructure and Environment Executive Agency” (CINEA), within the project “Condition Monitoring and Wide Bandgap Power Electronics - Leading Innovations for the European Energy Sector” (MoWiLife), call: HORIZON-CL5-2024-D3-01, Grant Agreement no. 101172657. Views and opinions expressed are those of the authors only and do not necessarily reflect those of the European Union or CINEA. Neither the European Union nor the granting authority can be held responsible for them.

Data availability

The data that has been used is confidential.

References

[1] P.N. Volpe, J. Pernot, P. Muret, F. Omnès, High hole mobility in boron doped diamond for power device applications, Appl. Phys. Lett. 94 (9) (2009), https://doi.org/10.1063/1.3086397.
[2] N. Donato, N. Rouger, J. Pernot, G. Longobardi, F. Udrea, Diamond power devices: state of the art, modelling, figures of merit and future perspective, J. Phys. D. Appl. Phys. (2020), https://doi.org/10.1088/1361-6463/ab4eab.
[3] J.P. Lagrange, A. Deneuville, E. Gheeraert, Activation energy in low compensated homoepitaxial boron-doped diamond films, Diam. Relat. Mater. vol. 7 (1998) 1390–1393, https://doi.org/10.1016/S0925-9635(98)00225-8, no. 9.
[4] A.T. Collins, A.W.S. Williams, The nature of the acceptor centre in semiconducting diamond, J. Phys. C Solid State Phys. 4 (13) (1971) 1789–1800, https://doi.org/10.1088/0022-3719/4/13/030.
[5] F. Fontaine, Calculation of the hole concentration in boron-doped diamond, J. Appl. Phys. 85 (3) (1999) 1409–1422, https://doi.org/10.1063/1.369272.
[6] H. Kato, T. Makino, S. Yamasaki, H. Okushi, n-type diamond growth by phosphorus doping on (001)-oriented surface, J. Phys. D. Appl. Phys. 40 (20) (2007) 6189–6200, https://doi.org/10.1088/0022-3727/40/20/S05.
[7] R.G. Farrer, On the substitutional nitrogen donor in diamond, Solid State Commun. 7 (9) (1969) 685–688, https://doi.org/10.1016/0038-1098(69)90593-6.
[8] M. Suzuki, High voltage diamond pin diodes: feasibility study on ultimate properties of diamond toward ultimate power devices, Oyo Buturi 85 (2016) 218–222.
[9] A. Nawawi, K.J. Tseng, Rusli, G.A.J. Amaratunga, H. Umezawa, S. Shikata, Design and optimization of planar mesa termination for diamond Schottky barrier diodes, Diam. Relat. Mater. 36 (2013) 51–57, https://doi.org/10.1016/J.DIAMOND.2013.04.009.
[10] P.-N. Volpe, et al., Extreme dielectric strength in boron doped homoepitaxial diamond, Appl. Phys. Lett. 97 (22) (2010), https://doi.org/10.1063/1.3520140.
[11] M. Kah, N. Donato, F. Udrea, Dynamic effects of incomplete ionization in edge terminations of diamond power devices, Diam. Relat. Mater. 160 (2025) 112994, https://doi.org/10.1016/j.diamond.2025.112994.
[12] N. Donato, F. Udrea, Static and dynamic effects of the incomplete ionization in superjunction devices, IEEE Trans. Electron Devices 65 (10) (2018) 4469, https://doi.org/10.1109/TED.2018.2867058.
[13] D.V. Lang, Deep-level transient spectroscopy: a new method to characterize traps in semiconductors, J. Appl. Phys. 45 (7) (1974) 3023–3032, https://doi.org/10.1063/1.1663719.
[14] M. Fregolent, et al., Deep levels and carrier capture kinetics in n-GaAsBi alloys investigated by deep level transient spectroscopy, J. Phys. D. Appl. Phys. 54 (34) (2021) 345109, https://doi.org/10.1088/1361-6463/ac0182.
[15] A.M. Zaitsev, Optical properties of diamond: a data handbook, Springer Science & Business Media, 2013.
[16] W.H. Guo, J.T. Huang, J. Hwang, Hysteresis loop in the current—voltage characteristic of Al/boron-doped polycrystalline diamond Schottky contact, Diam. Relat. Mater. vol. 6 (1997) 12–16, https://doi.org/10.1016/S0925-9635(96)00592-4, no. 1.
[17] A.S. Nikolenko, et al., Peculiarities of current transport in boron-doped diamond Schottky diodes with hysteresis in current–voltage characteristics, Diam. Relat. Mater. 143 (2024) 110897, https://doi.org/10.1016/j.diamond.2024.110897.
[18] P.G. Neudeck, C. Fazi, High-field fast-risetime pulse failures in 4H- and 6H-SiC pn junction diodes, J. Appl. Phys. 80 (2) (1996) 1219–1225, https://doi.org/10.1063/1.362922.
[19] M. Lades, W. Kaindl, N. Kaminski, E. Niemann, G. Wachutka, Dynamics of incomplete ionized dopants and their impact on 4H/6H-SiC devices, IEEE Trans. Electron Devices 46 (3) (1999) 598–604, https://doi.org/10.1109/16.748884.
[20] P. Muret, J. Pernot, T. Teraji, T. Ito, Deep levels in homoepitaxial boron-doped diamond films studied by capacitance and current transient spectroscopies, Phys. Status Solidi A 205 (9) (2008) 2179–2183, https://doi.org/10.1002/pssa.200879725.
[21] P. Muret, P.N. Volpe, J. Pernot, F. Omnès, Hole traps profile and physical properties of deep levels in various homoepitaxial diamond films studied by isothermal and deep level transient spectroscopies, Diam. Relat. Mater. 20 (5–6) (2011) 722–725, https://doi.org/10.1016/j.diamond.2011.03.013.
[22] H. Okushi, Y. Tokumaru, Isothermal capacitance transient spectroscopy, Jpn. J. Appl. Phys. 20 (S1) (1981) 261, https://doi.org/10.7567/JJAPS.20S1.261.
[23] Z. Wang, X. Chen, F.-F. Ren, S. Gu, J. Ye, Deep-level defects in gallium oxide, J. Phys. D. Appl. Phys. 54 (4) (2021) 043002, https://doi.org/10.1088/1361-6463/abbeb1.
[24] N. Modolo, et al., Trap-state mapping to model GaN transistors dynamic performance, Sci. Rep. 12 (1) (2022) 1755, https://doi.org/10.1038/s41598-022-05830-7.
[25] M. Fregolent, et al., Advanced defect spectroscopy in wide-bandgap semiconductors: review and recent results, J. Phys. D. Appl. Phys. 57 (43) (2024) 433002, https://doi.org/10.1088/1361-6463/ad5b6c.
[26] D.K. Schroder, Semiconductor Material and Device Characterization, in: Semiconductor Material and Device Characterization, 3rd ed., Wiley, Tempe, AZ, 2005 https://doi.org/10.1002/0471749095.fmatter.
[27] S.M. Sze, K.K. Ng, Physics of semiconductor devices, Wiley-Interscience, 2007.
[28] M. Willatzen, M. Cardona, N.E. Christensen, Linear muffin-tin-orbital and $\mathbf{k}\cdot\mathbf{p}$ calculations of effective masses and band structure of semiconducting diamond, Phys. Rev. B 50 (24) (1994) 18054–18059, https://doi.org/10.1103/PhysRevB.50.18054.
[29] M. Schreck, et al., Charge carrier trapping by dislocations in single crystal diamond, J. Appl. Phys. 127 (12) (2020), https://doi.org/10.1063/1.5140662.
[30] T. Shimomura, Y. Kubo, J. Barjon, N. Tokuda, I. Akimoto, N. Naka, Quantitative relevance of substitutional impurities to carrier dynamics in diamond, Phys. Rev. Mater. 2 (9) (2018), https://doi.org/10.1103/PhysRevMaterials.2.094601.
[31] O.S. Elsherif, K.D. Vernon-Parry, J.H. Evans-Freeman, P.W. May, Effect of doping on electronic states in B-doped polycrystalline CVD diamond films, Semicond. Sci. Technol. 27 (6) (2012) 065019, https://doi.org/10.1088/0268-1242/27/6/065019.
[32] A.C. Wang, C.T. Sah, New method for complete electrical characterization of recombination properties of traps in semiconductors, J. Appl. Phys. 57 (10) (1985) 4645–4656, https://doi.org/10.1063/1.335501.
[33] L.F. Makarenko, J.H. Evans-Freeman, Application of DLTS and Laplace-DLTS to defect characterization in high-resistivity semiconductors, Phys. B Condens. Matter 401–402 (2007) 666–669, https://doi.org/10.1016/j.physb.2007.09.047.
[34] P. Muret, J. Pernot, A. Kumar, L. Magaud, C. Mer-Calfati, P. Bergonzo, Deep hole traps in boron-doped diamond, Phys. Rev. B 81 (23) (2010) 235205, https://doi.org/10.1103/PhysRevB.81.235205.

[35] J.P. Goss, et al., Deep hydrogen traps in heavily B-doped diamond, Phys. Rev. B Condens. Matter Mater. Phys. 68 (23) (2003), https://doi.org/10.1103/PhysRevB.68.235209.
[36] A. Kumar, J. Pernot, A. Deneuville, L. Magaud, Ab initio study of boron-hydrogen complexes in diamond and their effect on electronic properties, Phys. Rev. B Condens. Matter Mater. Phys. 78 (23) (2008), https://doi.org/10.1103/PhysRevB.78.235114.
[37] T. Wosiński, Evidence for the electron traps at dislocations in GaAs crystals, J. Appl. Phys. 65 (4) (1989) 1566–1570, https://doi.org/10.1063/1.342974.
[38] T. Figielski, Recombination at dislocations, Solid State Electron. 21 (11–12) (1978) 1403–1412, https://doi.org/10.1016/0038-1101(78)90216-2.
[39] P. Muret, J. Pernot, T. Teraji, T. Ito, Near-surface defects in boron-doped diamond schottky diodes studied from capacitance transients, Appl. Phys. Express 1 (3) (2008) 0350031–0350033, https://doi.org/10.1143/APEX.1.035003.
[40] P. Muret, et al., Electrically active defects in boron doped diamond homoepitaxial layers studied from deep level transient spectroscopies and other techniques, *Physica Status Solidi (A) Applications and Materials* Science 206 (9) (2009) 2016–2021, https://doi.org/10.1002/pssa.200982218.